



Discovery of 3,6-disubstituted-imidazo[1,2-*a*]pyridine derivatives as a new class of CLK1 inhibitors

Yun Zhang^{a,c,1}, Anjie Xia^{a,1}, Shiyu Zhang^{b,1}, Guifeng Lin^a, Jingming Liu^a, Pei Chen^b,
Bo Mu^{a,d}, Yan Jiao^a, Wenwen Xu^b, Mingxin Chen^a, Linli Li^{b,*}

^a State Key Laboratory of Biotherapy and Cancer Center, West China Hospital, Sichuan University, Chengdu 610041, Sichuan, China

^b Key Laboratory of Drug Targeting and Drug Delivery System of Ministry of Education, West China School of Pharmacy, Sichuan University, Sichuan 610041, China

^c Macular Disease Research Laboratory, Department of Ophthalmology, West China Hospital, Sichuan University, Sichuan 610041, China

^d Basic Medical College of North Sichuan Medical College, Nanchong 637000, Sichuan, China

ARTICLE INFO

Keywords:

CLK1
Small molecule inhibitor
Structure-activity relationship
Autophagy

ABSTRACT

Inhibition of cdc2-like kinase1 (CLK1) could efficiently induce autophagy and it has been thought as a potential target for treatment of autophagy-related diseases. Herein we report the discovery of a series of 3,6-disubstituted-imidazo[1,2-*a*]pyridine derivatives as a new class of CLK1 inhibitors. Among them, compound **9e** is the most potent one, which exhibits an IC₅₀ value of 4 nM against CLK1 kinase. *In vitro*, this compound reduces the phosphorylation level of the typical downstream substrates of CLK1 and affects their subcellular redistribution. Further study indicates that **9e** is efficient to induce autophagy. Overall, this study provides a promising lead compound for drug discovery targeting CLK1 kinase.

Introduction

Autophagy is a mechanism conserved among eukaryotes by which the cells engulf cellular material in vesicles formed autophagosomes which fuse with lysosomes into autolysosomes for degradation to maintain homeostasis and protect cells from death^{1–3}. Autophagy can degrade long-lived proteins, misfolded proteins, and damaged organelles⁴. Dysfunction of autophagy has been shown to be associated with many diseases, such as cancer, infectious, neurodegenerative, and cardiovascular disease^{5–9}. Many protein kinases have been reported to participate in autophagy process regulation, one of them namely cdc2-like kinase1 (CLK1), which plays an important role in alternative splicing regulation of pre-mRNA by phosphorylation of the serine-arginine-rich (SR) protein^{10,11}. Previous studies revealed the inhibition of CLK1 could efficiently induce autophagy through the mTOR/PI3K pathway^{12,13}. Currently, several CLK1 small molecular inhibitors have been reported^{14–18}, but few of them were related to autophagy inducers¹⁷. Thus, discovering more CLK1 inhibitors with new scaffolds for additional treatment options for autophagy-related diseases has attracted much attention.

In the effort to seek potent CLK1 inhibitors, we performed a

molecular docking based virtual screening (VS) against SPECS and our in-house compound database (for detail, see Fig. S1), which gave a hit compound, (*S*)-6-(1-methyl-1*H*-pyrazol-4-yl)-*N*-(1-phenylethyl)-imidazo[1,2-*a*]pyridine-3-carboxamide (**E242**, Fig. 2). This compound showed moderate inhibitory activity against CLK1 (IC₅₀ = 296 nM) and required further optimization to improve its potency. The subsequent structural optimization was focused on two regions of **E242** (region A and region B, Fig. 1). Various substituents were used to replace these two regions, and a total of 25 new 3,6-disubstituted-imidazo[1,2-*a*]pyridine derivatives were synthesized.

To examine the influence of chiral benzylamine substituents (region A, R¹) on the bioactivity, we first fixed region B as the original 1-methyl-1*H*-pyrazol-4-yl group and varied the R¹ group substituents. The synthetic routes for compounds **6a–l** are depicted in Scheme 1. Briefly, treatment of commercially available **1** with DMF-DMA resulted in the formation of **2**, which was cyclized with ethyl 2-bromoacetate to obtain **3**. Suzuki coupling between **3** and 1-methyl-4-pyrazole boronic acid pinacol ester delivered intermediate **4a**, which was then hydrolyzed to offer the corresponding acid **5a**. Target compounds **6a–l** were finally generated by a condensation reaction of **5a** and various amines.

The chemical structures and bioactivities of compounds **6a–l** are

* Corresponding author.

E-mail address: lilinli@scu.edu.cn (L. Li).

¹ These authors contributed equally to this work.

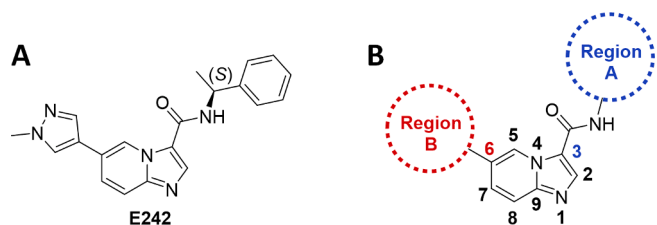


Fig. 1. (A) Chemical structure of E242. (B) Focuses of the structural modification.

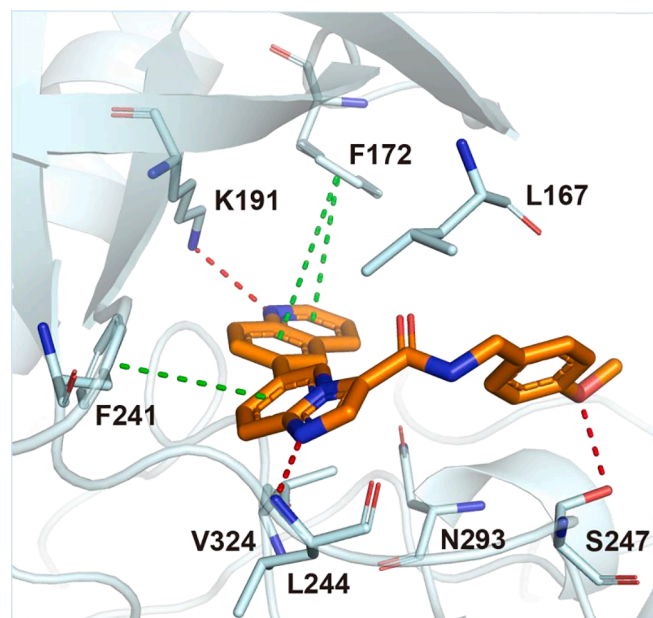


Fig. 2. Predicted binding mode of 9e with CLK1 (the CLK1 structure was taken from PDB entry 5X8I).

given in Table 1. Because E242 contains an *S* configuration 1-phenethyl group at the R^1 position, we first examined the bioactivity of its enantiomer 6a with an *R* configuration 1-phenethyl group. 6a displayed an obvious improvement in CLK1 inhibitory potency, indicating that the *R* configuration 1-phenethyl group is more favorable than the corresponding *S* configuration at the R^1 position.

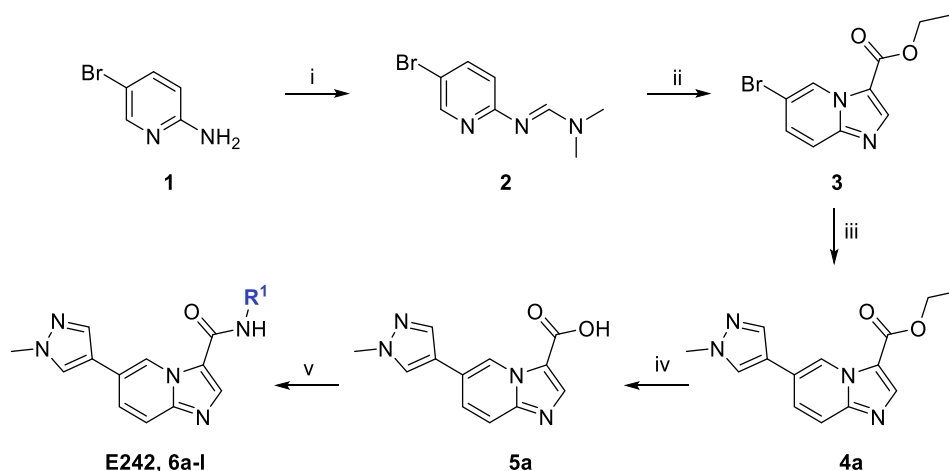
Next, we introduced methoxyl or chlorine in the C4 position at phenyl group, delivered potency enhanced *R* configuration compounds 6c and 6e, and potency decreased *S* configuration compounds 6b and 6d, further confirmed that the *R* configuration 1-phenethyl groups are preferred at the R^1 position. Then, we removed the chiral methyl on 1-phenethyl group and synthesized 5 non-chiral compounds (6f-j). Among them, 6f, which with a para-methoxybenzyl group, further increased the activity against CLK1 kinase. Finally, we replaced the benzyl group with smaller substitution groups (6k and 6l), and the two generated compounds showed reduced bioactivity. Therefore, it seems that para-methoxybenzyl is the best choice for R^1 .

In the second step, to explore the effect of the substituent at region B (R^2), we installed different subgroups, including pyridyl, substituted five-membered heterocyclic rings, and bicyclic aromatic groups in this position (R^2) and fixed region A as the optimal para-methoxybenzyl group. Another 5 new compounds (9a-e) were then synthesized. Scheme 2 illustrates the synthetic routes of these compounds. Intermediates 3 was readily prepared as depicted above. Hydrolyzation of 3 delivered acid 7, which then reacted with 4-methoxybenzylamine gave intermediate 8. Suzuki coupling of 8 with commercially available aromatic boric acid (or ester) yielded products 9a-e.

The chemical structures and bioactivities of compounds 9a-e are shown in Table 2, revealing that substitutions at region B substantially impacted the activity. Replacement of the 1-methyl-1H-pyrazol-4-yl group with pyridin-4-yl group maintained the potency (9a vs 6f), but introduction of 3,5-dimethylisoxazol-4-yl (9b), benzo[*d*]oxazol-5-yl (9c) and naphthalen-2-yl (9d) at R^2 position resulted in significantly decreased or completely absent CLK1 activities. Compound 9e, which has a quinolin-6-yl moiety at the R^2 position displayed the best performance, with an IC_{50} value of 4 nM against CLK1. Collectively, quinolin-6-yl group may be the best choice for region B.

In the last step, to examine whether para-methoxybenzyl group is still optimal when region B is fixed as quinolin-6-yl a moiety, we prepared eight compounds with different substituents at region A (10a-h). The synthetic routes for these compounds are given in Scheme 3, which is similar to that in Scheme 1.

Table 3 shows the CLK1 inhibitory activities of compounds 10a-h. It can be seen that the introduction of chiral 1-phenethyl group at R^3 position resulted in no improvement of the potency, and again *S* configuration compounds 10a and 10c exhibited weaker potency compared with *R* configuration enantiomers 10b and 10d. Replacement of the para-methoxyl of 9e with para-ethoxyl or para-isopropoxyl led to the obvious loss in CLK1 inhibitory activity.

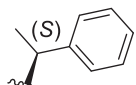
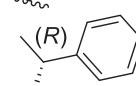
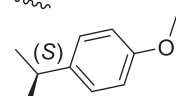
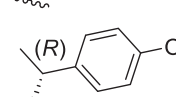
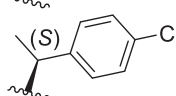
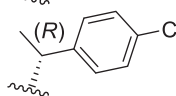
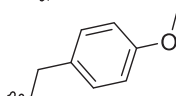
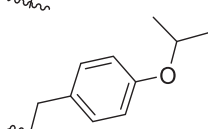
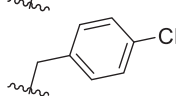
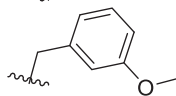
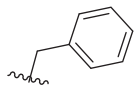
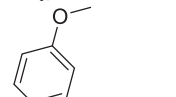


Scheme 1. Synthetic routes for compounds 6a-l, and E242. Reagents and conditions: (i) DMF-DMA, DMF 65 °C; (ii) NaHCO₃, ethyl 2-bromoacetate, DMF, 85 °C; (iii) 1-methyl-4-pyrazole boronic acid pinacol ester, PdCl₂(dppf), K₂CO₃, 1,4-dioxane/H₂O, 100 °C; (iv) LiOH·H₂O, THF/MeOH/H₂O, 60 °C; (v) substituted amine, EDCl, 1-Hydroxybenzotriazole, triethylamine, DCM, rt.

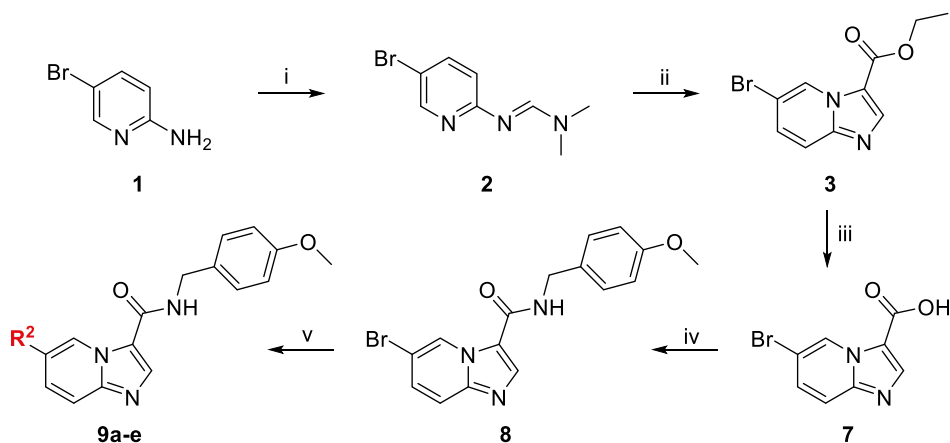
Table 1

Bioactivities of compounds **6a-l** and **E242**^a.



Compound	R ¹	IC ₅₀ (nM)	%Control @10 μM
E242		296	-7
6a		14	-14
6b		809	0
6c		8	-3
6d		399	12
6e		11	5
6f		6	-12
6g		8	0
6h		14	1
6i		11	1
6j		12	1
6k		7	3
6l	Methyl	23	1

^a IC₅₀ values were determined from Kinase Profiler of Eurofins. [ATP] = 10 μM.



Scheme 2. Synthetic routes for compounds **9a-e**. Reagents and conditions: (i) DMF-DMA, DMF 65 °C; (ii) NaHCO₃, ethyl 2-bromoacetate, DMF, 85 °C; (iii) LiOH·H₂O, THF/MeOH/H₂O, 60 °C; (iv) 4-methoxybenzylamine, EDCI, 1-Hydroxybenzotriazole, triethylamine, DCM, rt; (v) commercially available aromatic boric acid (or ester), PdCl₂(dppf), K₂CO₃, 1,4-dioxane/H₂O, 100 °C.

Table 2

Bioactivities of compounds **9a-e**^a.

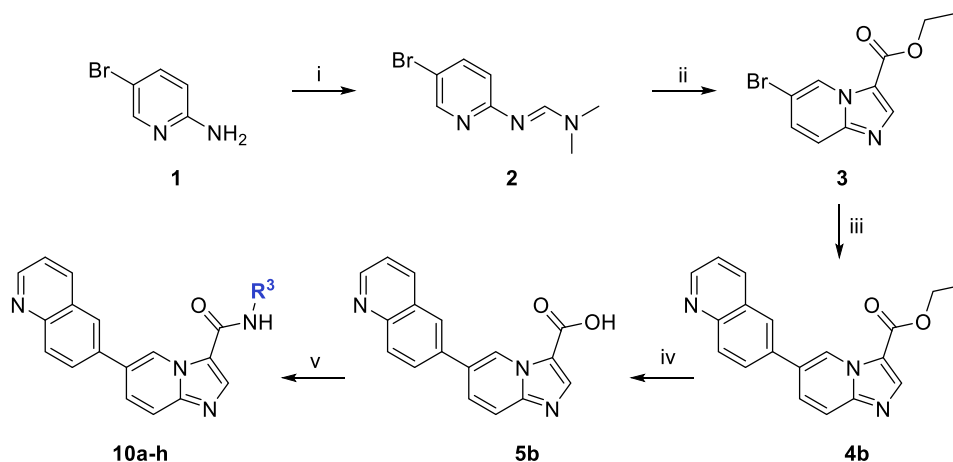
Compound	R ²	IC ₅₀ (nM)	%Control @10 μM
9a		13	-9
9b		>10000	59
9c		122	-5
9d		>10000	88
9e		4	2

^a IC₅₀ values were determined from Kinase Profiler of Eurofins. [ATP] = 10 μM.

(**10e-f**). The shift of methoxyl from para-position to meta-position also reduced the potency (**10g**). At last, Hydrazide **10h** was synthesized, which showed high bioactivity but still did not exceed **9e** in terms of potency.

Then we used molecular docking to predict the binding model of **9e** and CLK1. As shown in Fig. 2, **9e** suitably occupies the ATP binding pocket of CLK1. The nitrogen atom of quinoline of **9e** forms one

hydrogen bond with Lys191. Another hydrogen bond is formed between the imidazo[1,2-*a*]pyridine nitrogen atom and Leu244 on the hinge. The oxygen atom of methoxyl also forms one hydrogen bond with Ser247, which might be the reason why para-methoxybenzyl is the best choice on 3-position of the scaffold. In addition, it is also obvious that the quinoline of **9e** forms a π-π stacking interaction with the benzene ring of Phe172, and the imidazo[1,2-*a*]pyridine scaffold formed a T-shape π-π



Scheme 3. Synthetic routes for compounds **10a-h**. Reagents and conditions: (i) DMF-DMA, DMF 65 °C; (ii) NaHCO₃, ethyl 2-bromoacetate, DMF, 85 °C; (iii) quinolin-6-ylboronic acid, PdCl₂(dppf), K₂CO₃, 1,4-dioxane/H₂O, 100 °C; (iv) LiOH·H₂O, THF/MeOH/H₂O, 60 °C; (v) substituted amine, EDCl, 1-Hydroxybenzotriazole, triethylamine, DCM, rt.

Table 3

Bioactivities of compounds **10a-h**^a.

Entry	R ³	IC ₅₀ (nM)	%Control @10 μM
10a		52	3
10b		6	-9
10c		44	0
10d		6	-3
10e		ND ^b	40
10f		ND ^b	48
10g		ND ^b	46
10h		5	-11

^a IC₅₀ values were determined from Kinase Profiler of Eurofins. [ATP] = 10 μM.

^b ND, not determined.

interaction with the benzene ring of CLK1 Phe241. These interactions explain the high potency of compound **9e**.

Overall, through the above structural optimization, a number of new CLK1 inhibitors were obtained. Among them, **9e** is the most potent one. Further studies were then performed on this compound.

Firstly, we tested the subcellular redistribution and the phosphorylation level of the SR proteins in cells, which are typical downstream substrates of CLK1. When CLK1 is inhibited, the SR proteins will be redistributed from the nucleoplasm as the active form to the storage form in the nuclear speckles and the phosphorylation level of SR

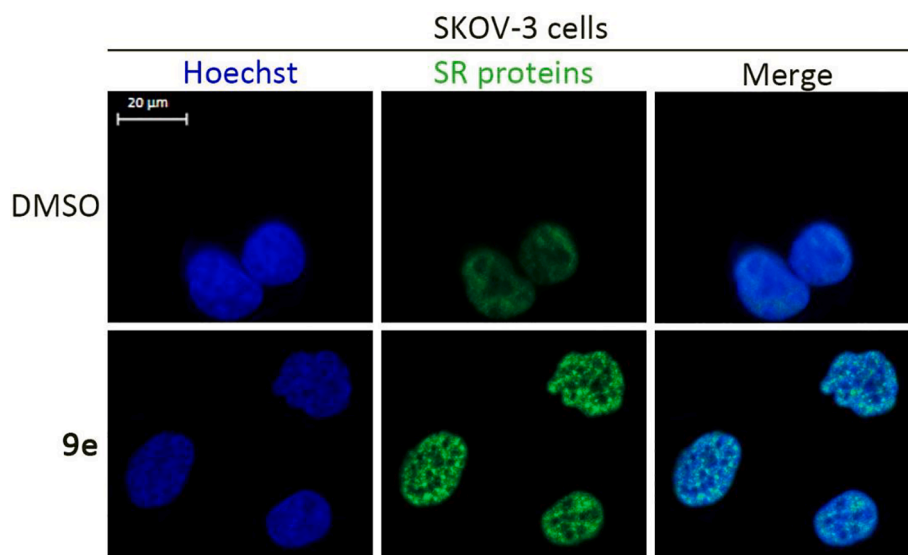


Fig. 3. Compound **9e** redistributed the location of SR proteins. SKOV-3 cells treated with compound **9e** (0.1 μM) or DMSO (0.1%) for 24 h were fixed and incubated with anti-SR proteins antibody (mAb1H4G7). The typical nuclear speckles and diffuse staining indicated the stored and active forms of SR proteins, respectively. Hoechst33342 was used to dye the nucleus. Scale bar: 20 μm .

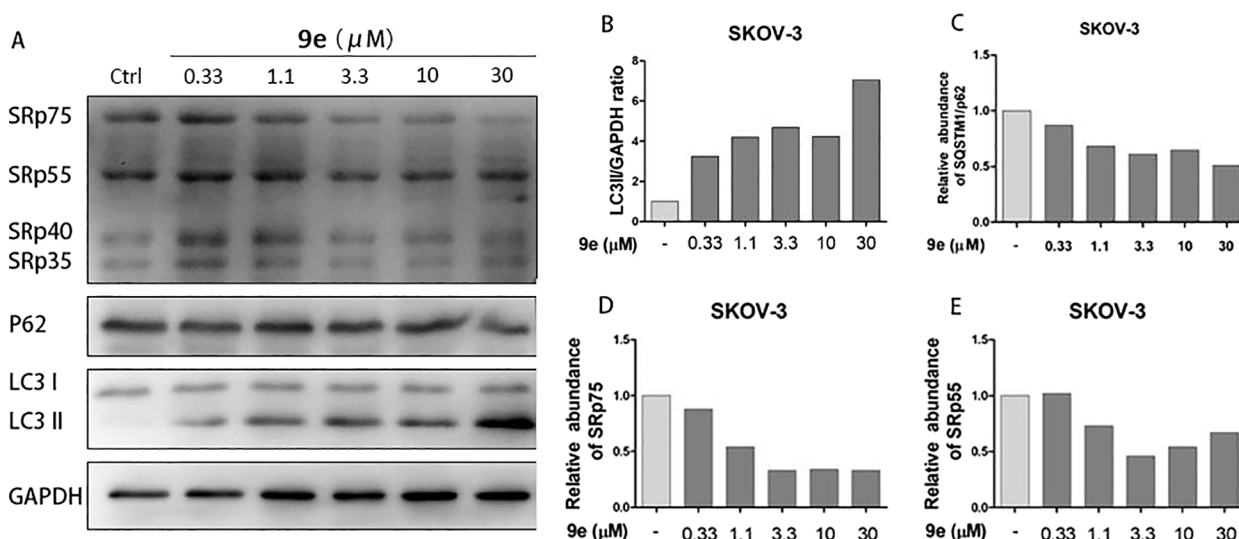


Fig. 4. Compound **9e** induced autophagy and increased autophagic flux in SKOV-3 cells. (A) Western blot analysis of the SR protein phosphorylation level, the LC3II/GAPDH ratio, and the SQSTM1/p62 protein expression in SKOV-3 cells treated with compound **9e** (0.33, 1.1, 3.3, 10, and 30 μM) for 24 h. (B-E) The quantification of immunoblot is shown in the right panel.

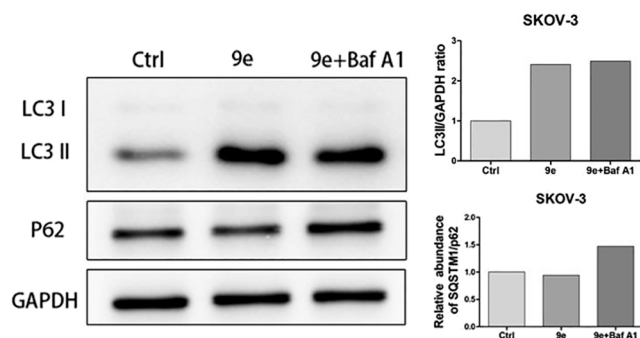


Fig. 5. Western blot analysis of the LC3II/GAPDH ratio and the SQSTM1/p62 protein expression after SKOV-3 cells were incubated with compound **9e** (10 μM) and Baf A1 (50 nM) individually or in combination for 24 h.

proteins will be decreased, both of these phenomena could be detected. Immunofluorescence was adopted to examine the distribution of SR proteins in SKOV3 cells (human ovarian cancer cell line), which represented whether the CLK1 activation could be inhibited by compound **9e**. As shown in Fig. 3, compound **9e** (0.1 μM) truly caused the obvious redistribution of SR proteins from the nucleoplasm to the nuclear speckles, which presented the speckled fluorescence, indicating the inhibition of CLK1 by compound **9e**. Furthermore, western blot assays were used to examine the phosphorylation level of SR proteins with or without compound **9e** treatment. The compound **9e** could decrease the level of SR proteins phosphorylation in a dose-dependent manner, including serine/arginine-rich splicing factor 4 (SRSF4, also known as SRp75), serine/arginine-rich splicing factor 6 (SRSF6, also known as SRp55), as shown in Fig. 4. Thus, we confirmed that compound **9e** is efficient to dose-dependently inhibit the activation of CLK1 in intact cells.

SKOV-3 (Ad-mRFP-GFP-LC3)

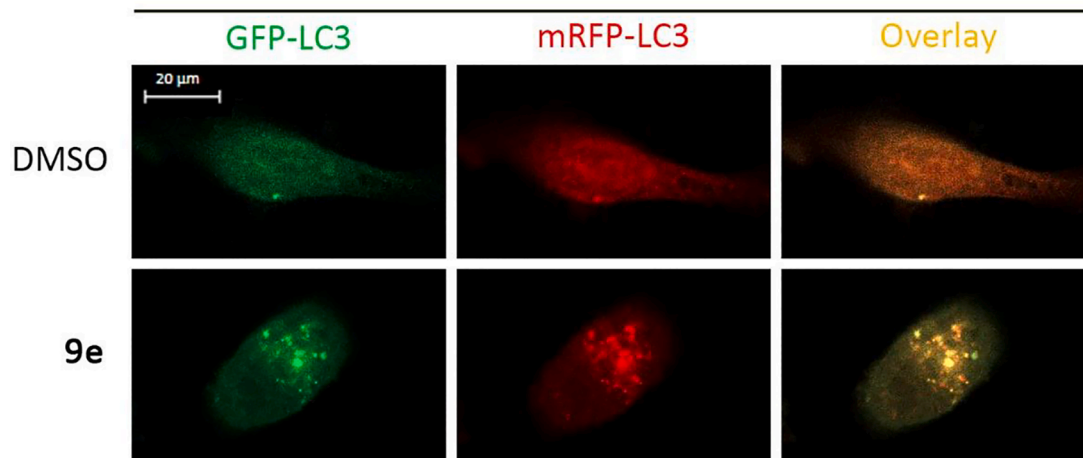


Fig. 6. Ad-mRFP-GFP-LC3-infected SKOV-3 cells were treated with **9e** (0.1 μ M) for 24 h and observed with confocal microscopy. Representative photographs are showed. Scale bar: 20 μ m. The overlap of green and red signals appears yellow which represents the formation of autophagosome.

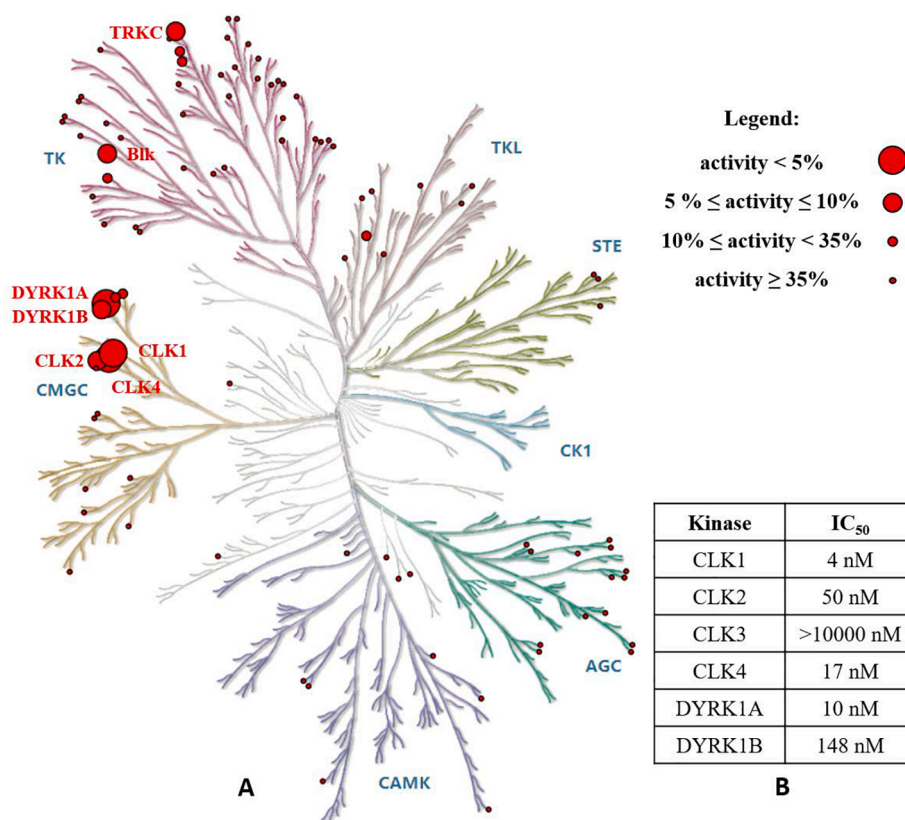


Fig. 7. (A) Kinase selectivity of **9e** shown on the human kinome dendrogram determined by the Kinase Profiler of Eurofins. (B) IC₅₀ value of **9e** on CLKs, DYRK1A and DYRK1B.

Secondly, the ability of compound **9e** to induce autophagy *in vitro* was examined in SKOV-3 cells. Western blot assays showed that compound **9e** could increase the level of LC3II protein (a marker of autophagosomes), as well as the ratio of LC3II to LC3I (a sensitive index of autophagy) in a dose-dependent manner. All of these demonstrated the ability of **9e** on autophagy induction (Fig. 4). Further, we infected the SKOV-3 cells with Ad-mRFP-GFP-LC3 (adenovirus-coding tandem GFP-mRFP-LC3). In confocal microscopy, compound **9e** could increase the number of yellow LC3 puncta colocalized with GFP and mRFP signals, compared with diffused yellow fluorescence in the control group. This represented the

LC3I was converted to LC3II and formed autophagosomes (Fig. 6). Therefore, we concluded that compound **9e** could efficiently induce the formation of autophagosome. For detecting the formation of autolysosome, we observed the number of red LC3 puncta (in mRFP signals only) which indicated the formation of autolysosomes fused with matured autophagosome and lysosome. After the treatment of the compound **9e**, the increased red LC3 puncta number confirmed the induction of autolysosomes formation (Fig. 6). The SQSTM1/p62 serves as a marker of autolysosomes to deliver autophagic substrate for degradation by autophagy. The degradation of SQSTM1/p62 induced by compound **9e** is

presented in Fig. 4. The V-ATPase inhibitor bafilomycin A1 (Baf A1) decreased the autophagosome-lysosome fusion by inhibiting lysosomal degradation. Inhibition of the lysosome with Baf A1 decreased the autophagic flux, which presented the high level of LC3II and SQSTM1/p62 (Fig. 5). Both of them indicated induction of autophagic flux by compound 9e, which were used to denote overall autophagic degradation. All of the above results demonstrated that compound 9e was an efficient inducer of autophagy targeting CLK1 kinase.

Finally, we tested 120 representative recombinant human protein kinases covering all kinase families to examine the selectivity of compound 9e (Fig. 7). Inhibition rates of 9e against these kinases were measured at 10 μ M concentration. As expected, CLK1 was the most potently inhibited kinase (IC_{50} = 4 nM). 9e also displayed considerable activity of CLK2 (IC_{50} = 50 nM) and CLK4 (IC_{50} = 17 nM), which are isoforms of CLK1. Except of CLKs, DYRK1A was the strongest off-target (IC_{50} = 10 nM), other potential off-targets are DYRK1B, Blk and TRKC. Of note is that 9e did not show obvious inhibitory activity against all other tested kinases, indicating a good selectivity (S score (5) = 0.025).

In summary, we obtained a new series of 3,6-disubstituted-imidazo[1,2-a]pyridine derivatives as CLK1 inhibitors. The most potent one, compound 9e, showed an IC_{50} value of 4 nM against CLK1. *In vitro*, compound 9e could induce autophagy efficiently in intact cells, change the subcellular redistribution, and inhibit the phosphorylation of SR proteins. Collectively, 9e could be a potential lead compound for further drug discovery of CLK1 target and treatment for autophagy-related diseases.

Declaration of Competing Interest

The authors declare that they have no known competing financial interests or personal relationships that could have appeared to influence the work reported in this paper.

Acknowledgements

This work was supported by the National Natural Science Foundation of China (21772130), China Postdoctoral Science Foundation (2020M683337), Post-Doctor Research Project, West China Hospital, Sichuan University (2020HXBH112, 2020HXBH120, 2020HXBH122), and 1.3.5 project for disciplines of excellence, West China Hospital, Sichuan University.

Appendix A. Supplementary data

Supplementary data to this article can be found online at <https://doi.org/10.1016/j.bmcl.2021.127881>.

References

- [1] Mizushima N. A brief history of autophagy from cell biology to physiology and disease. *Nat Cell Biol.* 2018;20:521–527. <https://doi.org/10.1038/s41556-018-0092-5>.
- [2] Levy JMM, Towers CG, Thorburn A. Targeting autophagy in cancer. *Nat Rev Cancer.* 2017;17:528–542. <https://doi.org/10.1038/nrc.2017.53>.
- [3] Nakatogawa H. Mechanisms governing autophagosome biogenesis. *Nat Rev Mol Cell Biol.* 2020;21:439–458. <https://doi.org/10.1038/s41580-020-0241-0>.
- [4] Ravikumar B, et al. Regulation of mammalian autophagy in physiology and pathophysiology. *Physiol Rev.* 2010;90:1383–1435. <https://doi.org/10.1152/physrev.00030.2009>.
- [5] Yamamoto K, et al. Autophagy promotes immune evasion of pancreatic cancer by degrading MHC-I. *Nature.* 2020;581:100–105. <https://doi.org/10.1038/s41586-020-2229-5>.
- [6] Matsuzawa-Ishimoto Yu, Hwang S, Cadwell K. Autophagy and inflammation. *Annu Rev Immunol.* 2018;36:73–101. <https://doi.org/10.1146/annurev-immunol-042617-053253>.
- [7] Bagherniya M, Butler AE, Barreto GE, Sahebkar A. The effect of fasting or calorie restriction on autophagy induction: a review of the literature. *Ageing Res Rev.* 2018; 47:183–197. <https://doi.org/10.1016/j.arr.2018.08.004>.
- [8] Guo F, Liu X, Cai H, Le W. Autophagy in neurodegenerative diseases: pathogenesis and therapy. *Brain Pathol.* 2018;28:3–13. <https://doi.org/10.1111/bpa.12545>.
- [9] Bravo-San Pedro JM, Kroemer G, Galluzzi L. Autophagy and mitophagy in cardiovascular disease. *Circ Res.* 2017;120:1812–1824. <https://doi.org/10.1161/CIRCRESAHA.117.311082>.
- [10] George A, Aubol BE, Fattat L, Adams JA. Disordered protein interactions for an ordered cellular transition: Cdc2-like kinase 1 is transported to the nucleus via its Ser-Arg protein substrate. *J Biol Chem.* 2019;294:9631–9641. <https://doi.org/10.1074/jbc.RA119.008463>.
- [11] Ninomiya K, et al. LncRNA-dependent nuclear stress bodies promote intron retention through SR protein phosphorylation. *Embo j.* 2020;39, e102729. <https://doi.org/10.15252/emboj.2019102729>.
- [12] Zhang Li, et al. Clk1-regulated aerobic glycolysis is involved in glioma chemoresistance. *J Neurochem.* 2017;142:574–588. <https://doi.org/10.1111/jnc.14096>.
- [13] Gu R, et al. Clk1 deficiency promotes neuroinflammation and subsequent dopaminergic cell death through regulation of microglial metabolic reprogramming. *Brain Behav Immun.* 2017;60:206–219. <https://doi.org/10.1016/j.bbi.2016.10.018>.
- [14] Petsalaki E, Zachos G. Clks 1, 2 and 4 prevent chromatin breakage by regulating the Aurora B-dependent abscission checkpoint. *Nat Commun.* 2016;7:11451. <https://doi.org/10.1038/ncomms11451>.
- [15] Tazarki H, et al. New pyrido[3,4-g]quinazoline derivatives as CLK1 and DYRK1A inhibitors: synthesis, biological evaluation and binding mode analysis. *Eur J Med Chem.* 2019;166:304–317. <https://doi.org/10.1016/j.ejmech.2019.01.052>.
- [16] Saldivia M, et al. Targeting the trypanosome kinetochore with CLK1 protein kinase inhibitors. *Nat Microbiol.* 2020;5:1207–1216. <https://doi.org/10.1038/s41564-020-0745-6>.
- [17] Sun Q-Z, et al. Discovery of Potent and Selective Inhibitors of Cdc2-Like Kinase 1 (CLK1) as a new class of autophagy inducers. *J Med Chem.* 2017;60:6337–6352. <https://doi.org/10.1021/acs.jmedchem.7b00665>.
- [18] Némec V, Hylšová M, Maier L, et al. Furo[3,2-b]pyridine: a privileged scaffold for highly selective kinase inhibitors and effective modulators of the hedgehog pathway. *Angw Chem Int Ed.* 2019;58:1062–1066. <https://doi.org/10.1002/anie.201810312>.